Accurate Imaging of a Moving Target in Shadow Regions with UWB Radar Using Doppler Effect

Shuhei Fujita, Takuya Sakamoto and Toru Sato
Graduate School of Informatics, Kyoto University
Yoshida-Honmachi, Sakyo-ku, Kyoto 606-8501, Japan
E-mail: tsato@kuee.kyoto-u.ac.jp

***Abstract*—This paper presents an imaging method for a target in blind areas of a room. We have developed an accurate imaging method for an indoor object in blind areas, but the estimated range of the imaging is restricted because of the mutual interference of indoor multi-path echoes [1]. In this paper, we extend this conventional method for a moving target and resolves the mutual interference using the Doppler effect. Numerical simulation shows that the proposed method achieves wide-range imaging of a target and accurately estimates target velocity.**

I. Introduction

Indoor surveillance systems are indispensable for maintaining a safe society. A system using radio waves is promising in surveillance systems because it has the potential to avoid some of the substantial limitations of camera-based systems. It has been reported that radio waves enable the detection of targets in hidden places where cameras cannot work. Existing communication infrastructure like WLAN stations has been employed for positioning purposes[2] [3]. Although these methods are capable of providing rough estimates of target locations in blind areas, the resolution is inadequate.

To obtain more accurate information, ultra-wide band (UWB) pulse radar is promising for surveillance imaging because of its high range resolution. Positioning methods using UWB pulse radar have been proposed for an environment with multi-path echoes such as the interior of a room[4] [5]. Combining the time-reversal (TR) [5] and interferometry [6] imaging methods, we proposed an accurate imaging method using multi-path echoes, which works even if the target is in blind areas[1].

However, this method provides a limited part of the target shape because only a small number of echoes are used for imaging due to mutual interference of the received echoes. In this paper, we resolve this problem by using the Doppler effect and assume a moving target. The proposed method calculates the Fourier Transform of the received signals and separates out the interference echoes in the frequency domain. A numerical simulation verifies that the proposed method extends the range of the estimated image and estimates the target velocity accurately.

II. System Model

Figure 1 shows the system model. We consider a two-dimensional case. The position is expressed with the parameter $\boldsymbol{r} = (x, y)$. The system is composed of an antenna array, a perfect-electric-conductor (PEC) target and a room configured as a known polygonal shape with PEC walls. The target with a velocity of $\boldsymbol{v}_{\mathrm{t}}$ is in the shadow regions, which are areas not visible from any location along the array antenna line. The region painted the darkest gray in Fig. 1 reperesents the shadow region in the system model. The location of the i-th antenna is expressed as $\boldsymbol{a}_i = (i\Delta x + x_0, y_0)$, where Δx is the interval of the array antenna. The antenna is assumed to have an ideally uniform beam pattern with a beam width of 180° and with the main lobe in the direction of the y axis.

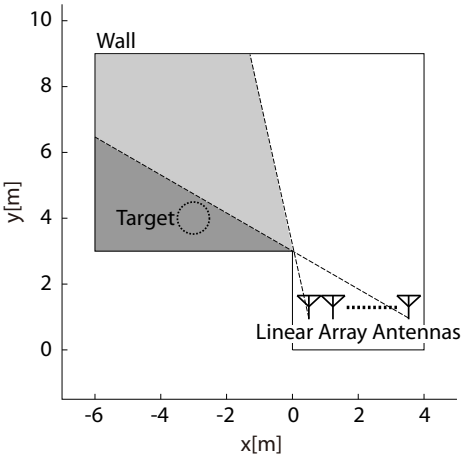

Fig. 1. System model.

Raised-cosine-shaped UWB pulses, with a center frequency of f_{c} and a bandwidth of B_{w}, are transmitted, and the echoes are received by the same antenna at a time interval of ΔT. $s_i(r, n\Delta T)\,(n = 0, \cdots, N)$ denotes the signal received at the antenna location $\boldsymbol{a}_i$ at time $n\Delta T$, where N is the total number of received signals and r is defined with time t and the speed of the radio wave c as $r = ct$. Note that the observation time of $N\Delta T$ is sufficiently short that $\boldsymbol{v}_{\mathrm{t}}$ is assumed to be constant during that time. The echoes received when the room is empty are subtracted from $s_i(r, n\Delta T)$, and a filter matched to the transmitted waveform is applied.

For convenience, mirror image antennas are introduced at symmetrical positions with respect to the room walls as in Fig. 2. Each multipath wave can be modeled with an imaginary echo from the corresponding mirror image antenna. The location of the j-th mirror image antenna for the i-th antenna

978-1-4577-0919-7/12/$26.00 ©2011 IEEE

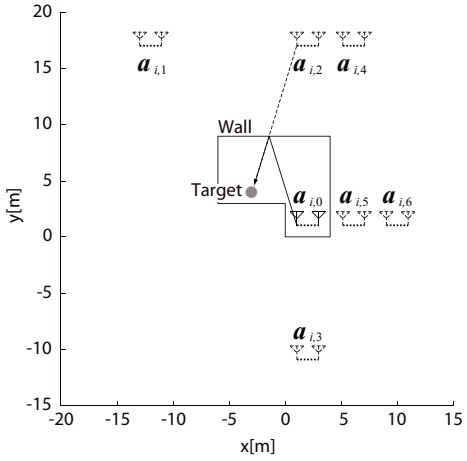

Fig. 2. Mirror image antennas.

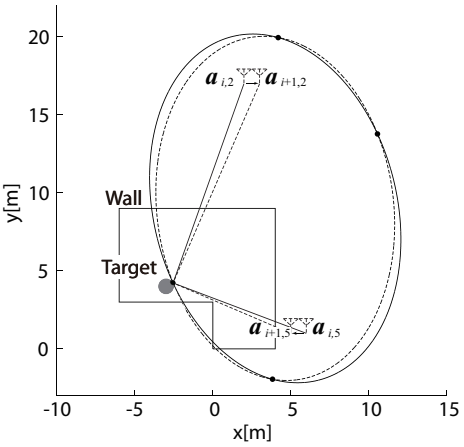

Fig. 3. Schematic of interferometry.

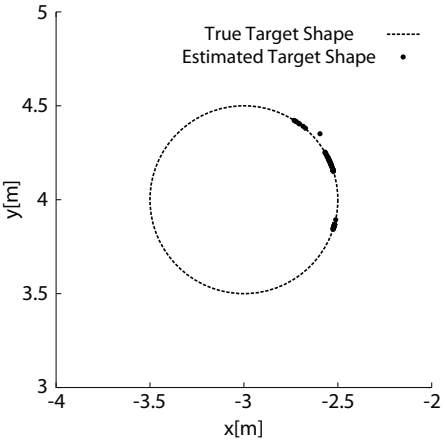

Fig. 4. Estimated image with conventional method.

is represented as $\boldsymbol{a}_{i,j}$.

Unless otherwise noted, $f_{\mathrm{c}} = 79.0\,\mathrm{GHz}$, $B_{\mathrm{w}} = 1.4\,\mathrm{GHz}$ $(x_0, y_0) = (0.1\,\mathrm{m}, 1.0\,\mathrm{m})$, $\Delta x = 0.1\,\mathrm{m}$, $M = 39$ and a circular target with a radius of $0.5\,\mathrm{m}$ located at $(-3.0\,\mathrm{m}, 4.0\,\mathrm{m})$ is assumed in this paper. The velocity of the target is $\boldsymbol{v}_{\mathrm{t}} = (0.50\,\mathrm{m/s}, 0.87\,\mathrm{m/s})$. An ideal environment without noise is assumed.

III. Interferometry Imaging in an Indoor Environment

The conventional method employs interferometry and TR imaging methods for a target in the indoor multi-path environment[1]. The image is provided as the superposition of the intersection points of two ellipses:

$$\begin{cases} |\boldsymbol{r} - \boldsymbol{a}_{i,j}| + |\boldsymbol{r} - \boldsymbol{a}_{i,k}| = r_{i,u}, & (1) \\ |\boldsymbol{r} - \boldsymbol{a}_{i+1,j}| + |\boldsymbol{r} - \boldsymbol{a}_{i+1,k}| = r_{i+1,v}, & (2) \end{cases}$$

where $r_{i,u}$ is the u-th range data extracted as the peak position of $s_i(r)$, which is the range from the antenna to the target. $r_{i,u}$ and $r_{i+1,v}$ satisfy the condition

$$|r_{i,u} - r_{i+1,v}| < \Delta R, \tag{3}$$

where ΔR is the length of the transmitted pulse in space. The schematic of this interferometry method is illustrated in Fig. 3, where an ellipse with foci $\boldsymbol{a}_{i,2}$ and $\boldsymbol{a}_{i,5}$, and another ellipse with foci $\boldsymbol{a}_{i+1,2}$ and $\boldsymbol{a}_{i+1,5}$ are used to calculate the target location.

The image includes many false image points across the room because incorrect combinations of antennas and range data are used in the estimation. Therefore, the conventional method removes the image points $\boldsymbol{r}_p$ satisfying the following condition:

$$|\boldsymbol{r}_p - \boldsymbol{r}_{\mathrm{tr}}| < \rho, \tag{4}$$

where $\boldsymbol{r}_p$ is the p-th image points, $\boldsymbol{r}_{\mathrm{tr}}$ is the location estimated using the TR imaging method and the parameter ρ is empirically determined.

Figure 4 shows the estimated image by applying this method to the system model shown in Fig. 1. The RMS error and the estimated range of the estimated shape are $0.47\,\mathrm{mm}$ and $7.0\,\%$. Although the result verifies that this method estimates the target shape accurately, only a small part of the target shape is provided because only a small amount of the range data is extracted owing to mutual interference of the received signals.

IV. Proposed Imaging Method

To resolve the problem mentioned above, the proposed method separates the received signals in the frequency domain using a Fourier transform. This approach is based on the principle that each received pulse has a unique value of the Doppler velocity v_{d} formulated as

$$\boldsymbol{v}_{\mathrm{t}} \cdot \boldsymbol{i} = v_{\mathrm{d}}, \tag{5}$$

where $\boldsymbol{i}$ is the incidence vector from the antenna to the target which is determined by the incidence angle from antenna to target.

In this section, we describe the procedure of the wide-range imaging method for an indoor object using the Doppler effect.

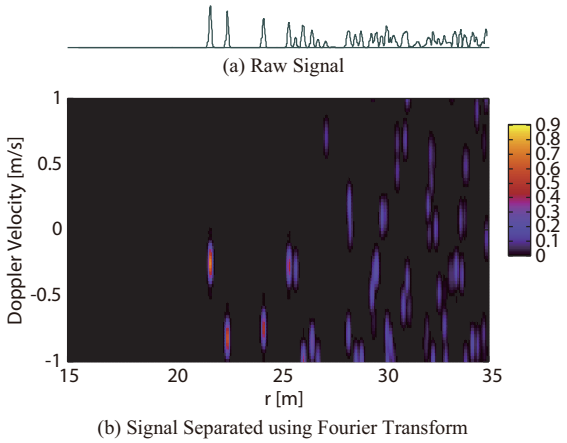

Fig. 5. Raw signal $s_{20}(r)$ and transformed signal $S_{20}(r, m\Delta f)$.

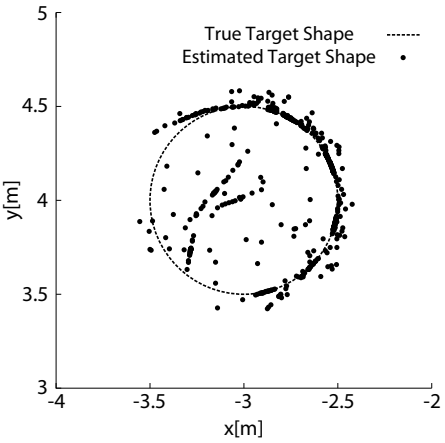

Fig. 6. Estimated image without false image reduction.

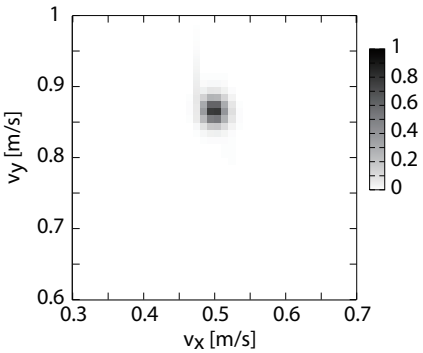

Fig. 7. Evaluation function $F(\boldsymbol{v})$.

A. Interferometry Imaging

We define the Fourier transform of $s_i(r, n\Delta T)$ as $S_i(r, m\Delta f)$. $(r_{i,u}, f_{i,u})$ is extracted as the peak position of $S_i(r, m\Delta f)$, where $f_{i,u}$ is the u-th frequency data. The image is obtained as the solutions of Eq. (1) and (2). In addition to Eq. (3), the combination of $r_{i,u}$ and $r_{i+1,v}$ is adopted by satisfying the condition

$$|f_{i,u} - f_{i+1,v}| < \Delta F/2, \tag{6}$$

where $\Delta F = 1/N\Delta T$ is the frequency resolution.

Figure 5 (a) shows $s_{20}(r, 31)$ and (b) shows the transformed signal $S_{20}(r, n\Delta f)$ in the system model shown in Fig. 1. The von Hann window is applied with the Fourier transform and $\Delta F = 100\,\mathrm{Hz}$. We set the other parameters $\Delta T = 3\,\mathrm{ms}$ and $N = 64$. $\Delta R = 0.2\,\mathrm{m}$ is calculated by $\Delta R = \mathrm{c}/B_\mathrm{w}$. It is confirmed that the received pulses are separated in the frequency domain.

The image estimated by this method is shown in Fig. 6. In this figure, the method reconstructs a wide range of the target boundary because the proposed method extracts more range data from the received signals than the conventional method. However, it also has many false image points due to the increment of the number of incorrect combinations of antennas and range data.

B. Velocity Estimation

To obtain a clear image, we propose an effective false image reduction algorithm using the Doppler frequency of the range data. In the first step, the proposed method estimates the target velocity from the image including the false image points. The velocity of the target $\boldsymbol{v}_{p,q}$ is calculated as the solution of the equations

$$\begin{cases} \boldsymbol{v}_{p,q} \cdot \boldsymbol{i}_p = v_p, & (7) \\ \boldsymbol{v}_{p,q} \cdot \boldsymbol{i}_q = v_q, & (8) \end{cases}$$

where the indexes p and q denote a specific image point, $\boldsymbol{i}_p$ is the unit vector parallel to the incident direction from the antenna to the p-th image point and v_p is the Doppler velocity for the p-th image point. The Doppler velocity v_d is obtained from the Doppler frequency f_d for $v_\mathrm{d} = -(\mathrm{c}/2f_\mathrm{c})f_\mathrm{d}$. First, the proposed method calculates $\boldsymbol{v}_{p,q}$ with all possible combinations of pairs of image points p and q. Note that $\boldsymbol{v}_{p,q}$ includes inaccurate velocity vectors because the image includes many false image points. To obtain accurate target velocity, the proposed method estimates the velocity of the target $\hat{\boldsymbol{v}}$ as

$$\hat{\boldsymbol{v}} = \arg\max_{\boldsymbol{v}} F(\boldsymbol{v}), \tag{9}$$

$$F(\boldsymbol{v}) = \left\{ \sum_{p,q} (a_p + a_q) G(\boldsymbol{v} - \boldsymbol{v}_{p,q}; \boldsymbol{\mu}, \sigma) \right\}, \tag{10}$$

where $G(\boldsymbol{v}; \boldsymbol{\mu}, \sigma)$ is a two-dimensional Gaussian function with a mean and standard deviation of $\boldsymbol{\mu} = \boldsymbol{0}$ and σ, and a_p is the amplitude of the pulse for the p-th image point. It is expected that F($\boldsymbol{v}$) has a high value at the position of true velocity because the image includes more true boundary points than false image points.

Figure 7 shows F($\boldsymbol{v}$) calculated by the image of Fig. 6. This figure verifies F($\boldsymbol{v}$) has a high value in the vicinity of $\boldsymbol{v} = (0.50\,\mathrm{m/s}, 0.87\,\mathrm{m/s})$ and the target velocity $\hat{\boldsymbol{v}}$ is accurately estimated.

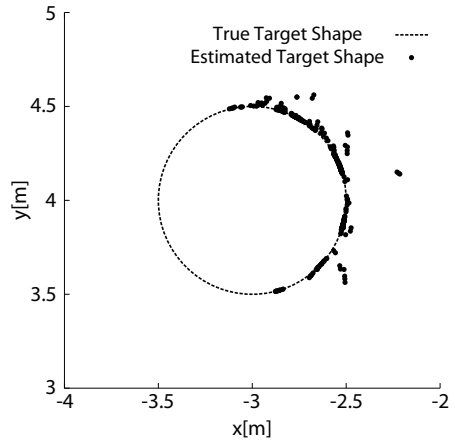

Fig. 8. Estimated image.

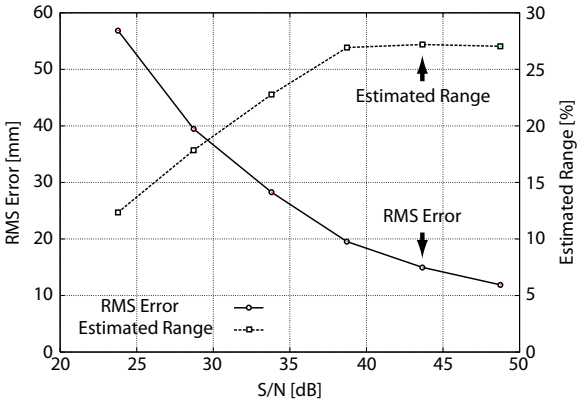

Fig. 9. RMS error and estimated range of the proposed method vs. S/N.

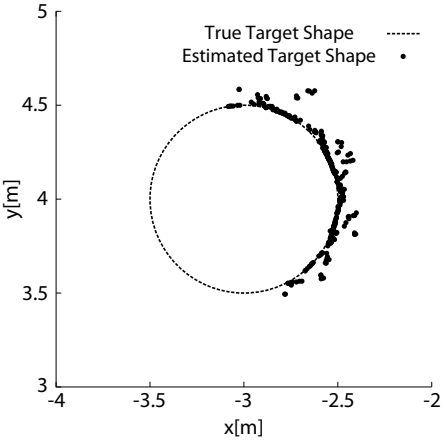

Fig. 10. Estimated image for $\mathrm{S/N} = 33.8\,\mathrm{dB}$.

C. False Image Reduction

In the second step of false image reduction, the proposed method removes the false image points using the estimated velocity. Using Eq.(5), the proposed method removes the image points that satisfy the following condition.

$$|v_p - \hat{\boldsymbol{v}} \cdot \boldsymbol{i}_p| > \eta\,|\hat{\boldsymbol{v}}|\,, \tag{11}$$

where η is an empirically determined parameter.

Moreover, the image satisfying the following condition is removed.

$$\min |\boldsymbol{r}_p - \boldsymbol{r}_{p'}| > \Delta r_{\mathrm{e}}\ (p \neq p'), \tag{12}$$

where Δr_{e} is an empirically determined parameter. This is because experience shows that the false image points are isolated from other points.

The estimated image after false image reduction is shown in Fig. 8, where we set $\rho = 0.8\,\mathrm{m}$, $\eta = 0.1$ and $\Delta r_{\mathrm{e}} = 0.02\,\mathrm{m}$. The root-mean-square (RMS) error and the estimated range of the proposed method are $10.5\,\mathrm{mm}$ and $23.1\,\%$ respectively. Although the RMS error of the proposed method deteriorates 20-fold compared with the conventional RMS error, the estimated range is extended about 3-fold.

V. Performance Evaluation

A. Noise Tolerance

This subsection discusses the imaging accuracy of the proposed method with noisy data assuming the same scenario as in the previous section. To produce a noisy signal numerically, white Gaussian noise is added to the raw signals. We define S/N as the ratio of the peak instantaneous signal power to the averaged noise power after applying the matched filter. The RMS error and estimated range of the estimated shape using the proposed method is shown in Fig. 9.

This figure shows that the RMS error and is relatively small, less than $40.0\,\mathrm{mm}$, and the estimated range is relatively large, more than $20.0\,\%$ for the $\mathrm{S/N} \geq 33.8\,\mathrm{dB}$. The image estimated in noisy environments is shown in Fig. 10 for $\mathrm{S/N} = 33.8\,\mathrm{dB}$. In Fig. 10, although there are inappropriate false points, most of the estimated points are located on the target surface, giving an accurate estimation of the image.

B. Performance Evaluation with Other Models

This subsection discusses the performance of the proposed method with different models. We apply the proposed method to the two system models shown in Figs. 11 and 12.

Figures 13 and 14 shows the images obtained from the models shown in Figs. 11 and 12. The estimation RMS error and estimated range are $2.04\,\mathrm{mm}$ and $29.8\,\%$, and $3.28\,\mathrm{mm}$ and $5.09\,\%$, respectively. In the system model shown in Fig. 11, the estimated range of the proposed method is extended about 3-fold compared with the conventional method and the RMS error of the proposed method is virtually the same as for the conventional method. In the system model shown in Fig. 12, the estimated range of the proposed method is extended about 1.5-fold compared with the conventional method and the RMS error of the proposed method improves 10-fold. These results verify that the region containing images is extended compared with the conventional interferometry method because the proposed method uses more multi-path echoes for imaging.

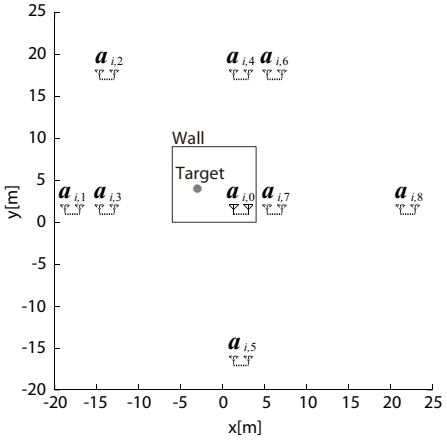

Fig. 11. System model B without shadow regions.

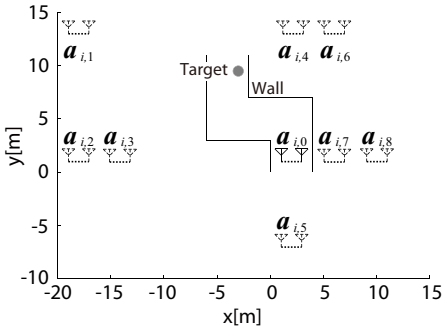

Fig. 12. System model C modeling a corner of a hallway.

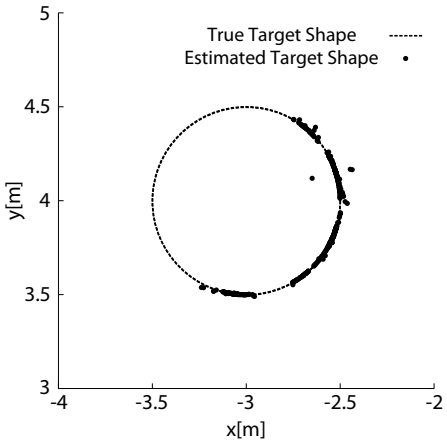

Fig. 13. Estimated image for system model B.

VI. Conclusions

This paper proposed a wide-range imaging method for a moving target in a shadow region. Numerical simulation verified that the proposed method separates the received signals in the frequency domain and accurately estimates the target shape and velocity. Moreover, we confirmed the proposed method works in several room shapes.

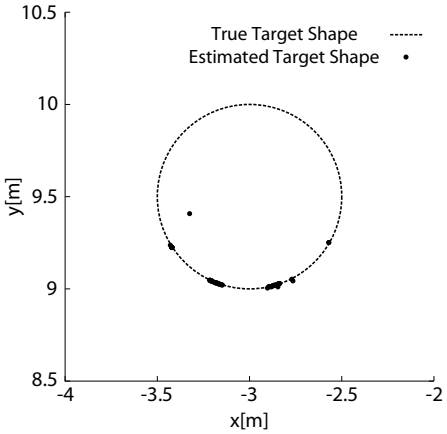

Fig. 14. Estimated image for system model C.

References

[1] S. Fujita, T. Sakamoto and T. Sato, "2-Dimensional Accurate Imaging with UWB Radar Using Indoor Multipath Echoes for a Target in Shadow Regions," IEICE Trans. Commun., vol. E94-B, pp. 2366–2374, 2011.

[2] S. Ikeda, H. Tsuji, and T. Ohtsuki, "Indoor event detection with Eigenvector spanning signal subspace for home or office security, " IEICE Trans. Commun., vol. E92-B, pp. 2406–2412, 2009.

[3] K. Pahlavan, F. O. Akgul, M. Heidari, A. Hatami, J. M. Elwell, and R. D. Tingley, "Indoor geolocation in the absence of direct path," IEEE Wireless Communications, vol. 13, no. 6, pp. 50–58, 2006.

[4] P. Meissner, T. Gigl, and K. Witrisal, "UWB Sequential Monte Carlo Positioning using Virtual Anchors " International Conference on Indoor Positioning and Indoor Navigation, pp. 355–364, 2010.

[5] Y. Jin, J. M. F. Moura, Y. Jiang, D. D. Stancil and A. G. Cepn, "Time Reversal Detection in Clutter: Additional Experimental Results " IEEE Trans. Aero. Electron. vol. AES-47, pp. 140–154, 2011.

[6] D. Massonet and K. L. Feigl, "Radar interferometry and its applica-tions to changes in the Earth's surface, " Rev. Geophys., vol. 36, no. 4, pp. 441–500, 1998.